Understanding the Effect of Salt Concentrations on Fast Charging Performance of Li-ion Cells

Xianyang Wu[a,b,c], Lin Ma[d,e] Jue Liu [c], Kejie Zhao[b], David L. Wood, III[a], Zhijia Du[a,z],

a Electrification and Energy Infrastructures Division, Oak Ridge National Laboratory, Oak Ridge, TN 37830, USA

b School of Mechanical Engineering, Purdue University, West Lafayette, IN 47907, USA

c Neutron Scattering Division, Oak Ridge National Laboratory, Oak Ridge, TN 37830, USA

d Department of Mechanical Engineering and Engineering Science, The University of North Carolina at Charlotte, Charlotte, NC 28223, USA

e Vehicle Energy & Safety Laboratory (VESL), North Carolina Motorsports and Automotive Research Center, The University of North Carolina at Charlotte, Charlotte, NC 28223, USA

-corresponding to Zhijia Du (duz1@ornl.gov, +1-(865)574-7519)

Abstract

Different lithium salt (lithium bis(fluorosulfonyl) imide (LiFSI)/$LiPF_6$ 9/1 mole ratio) concentrations in carbonate electrolyte were studied on the fast charging performance of $LiNi_{0.6}Mn_{0.2}Co_{0.2}O_2$ (NMC622)/graphite pouch cells. The cells with electrolyte concentration from 0.75 M to 1.50 M showed similar fast charging capabilities. Further increase of the concentration to 1.75 M and 2.00 M decreased the attainable capacity in fast charging. In the long-term cycling test, the capacity retention after 200 fast charging cycles increased with the increase of salt concentration in electrolyte. Cells with 1.5 M electrolyte showed the best overall performance in fast charging capacity and long-term cycling. Li plating were observed in the cells with 0.75 M, 1.00 M and 1.25 M electrolyte. It was improved with greatly reduced Li plating area in 1.50 M, and no Li plating at all in 1.75 M and 2.00 M electrolyte. Post-mortem analysis such as neutron powder diffraction (NPD) and X-ray photoelectron spectroscopy (XPS) were used to characterize the electrode after cycling. It suggests that electrolyte concentration needs to be optimized for a given cell configuration with specific electrode and loading.

Introduction

Lithium-ion batteries (LIBs), since its successful commercialization in 1991 by Sony, have greatly changed our daily life, from consumer electronics to battery electrical vehicles (BEVs). Further research and development of LIBs are vital for the energy evolution from fossil fuel energy to renewable energy and the realization carbon neutralization by 2060. These efforts aim critical goals such as higher energy density, longer lifetime, improved safety feature and advanced fast charging capabilities.

Although the cost of LIBs for BEVs has dropped greatly in the last 10 years, BEV market is still a small portion of the light-duty vehicle sales annually. It has been identified that the ability for BEVs to fast charge is a gap to wider BEV adoption [1]. High power Li-ion cells with relatively thin electrode thickness (areal loading < 2 mAh/cm^2) can be charged to > 80% capacity within 15 minutes. However, thinner electrodes can lead to increased battery cost significantly [1]. Increasing electrode thickness can effectively increase cell energy density [2]. The caveat is, however, Li-ion cells with thick electrodes cannot be readily fast charged. Li plating at the graphite anode remains unpreventable and becomes the greatest challenge for extreme fast charging (XFC), thus hindering the wider adaptation of BEVs. Typically, the limitation of Li ion mass transport in electrolyte leads to high polarization in cells with thick electrodes. Under higher charging rates, the electrochemical potential at the graphite anode drops below 0 V (vs. Li^+/Li) and thus triggers Li plating [3–5].

Electrolyte development has been identified to be important to enable fast charging for high energy density Li-ion cells [6–9]. Electrolyte typically consists of Li salt, solvent and additives. The description of Li ion transport phenomena in organic solvents stemmed from the general elaboration of mass and heat transport in organic media by Newman and Thomas-Alyea [10]. Du et al have discovered lithium bis(fluorosulfonyl) imide (LiFSI) can provide better fast charging performance than lithium hexafluorophosphate ($LiPF_6$) due to its higher ionic conductivity and higher Li ion transference number [7,11]. Another factor for Li salt optimization is the Li ion concentration. Previous studies suggest there are strong correlations between Li salt molarity and electrochemical performance [12–15]. Valøen et al. systematically studied Li ion transport properties with increasing $LiPF_6$ molarity, and revealed that Li ion transference number remained constant despite of increasing salt concentration [12]. Wang et al. probed the rate performance for

$LiCoO_2$−graphite pouch cells, and found the rate performance was improved with the increase of salt molarity from 0.5 M to 2 M $LiPF_6$ [13]. Xiong et al. studied the ethylene carbonate (EC)-free ethyl methyl carbonate (EMC)-based electrolytes with different concentrations of $LiPF_6$ (0.3 M–2 M), and suggested that 1.5 M $LiPF_6$ should be used to optimize cell performance [16].

In this study, different Li salt concentrations of (LiFSI/$LiPF_6$ 9/1 mole ratio) in carbonate electrolyte were used for fast charging test in $LiNi_{0.6}Mn_{0.2}Co_{0.2}O_2$ (NMC622)/graphite pouch cells. With the increase of Li salt concentration, Li plating was alleviated, and cycling performance was improved. By comparing the attainable capacity during fast charging and long-term cycling performance, 1.50 M electrolyte showed the most promising result.

Experiments

Preparation of electrolytes: Electrolyte was prepared in Ar-filled glove box. LiFSI (HSC Corp.) and $LiPF_6$ (Soulbrain MI) with mole ratio of 9/1 were dissolved into solvent mixture of EC, EMC and dimethyl carbonate (DMC) (all from Soulbrain MI) at a ratio of 40/30/30 wt%. 6 different concentrations were prepared at 0.75 M, 1.00 M, 1.25 M, 1.50 M, 1.75 M, 2.00 M. Electrolyte conductivity was measured using a conductivity cell (Cole-Parmer). The conductivity cell was calibrated using standard KCl solutions. The conductivities were measured using electrochemical impedance spectroscopy from 10 Hz to 1 MHz with a 6 mV perturbation voltage using a potentiostat (Bio-Logic) [7].

Preparation of pouch cells: The NMC622 and graphite electrodes are prepared at the DOE Battery Manufacturing R&D Facility (BMF) at Oak Ridge National Laboratory. The cathode consists of 94 wt% NMC622 (Targray), 3 wt% carbon black (Denka Li-100) and 3 wt% polyvinylidene fluoride (PVDF, Solvay 5130), with an area loading of 3.00 (±0.05) mAh/cm^2 and porosity of 30% after calendering. The graphite anode consists of 94 wt% graphite (Superior Graphite 1520T), 1 wt% carbon black (Timical C65) and 5 wt% polyvinylidene fluoride (PVDF, Kureha 9300). The area loading was 3.40 (±0.05) mAh with a porosity of 30% after calendering. The same amount of electrolyte (by volume) with different concentrations were filled into the pouch cells. Electrolyte volume factor is 1.2, which is defined as the supplied electrolyte volume divided by the total cell pore volume (the sum of pore volumes in anode, cathode, and separator). The pouch cells were multilayered with cathodes and anodes stacking together separated by separators (Celgard® 2325). The cells were placed in between two Al plates and bolted down with a pressure of 4 psi on the

cells. The nominal capacity of the pouch cells is 520 (±9) mAh. 3 cells for each electrolyte were prepared to ensure the repeatability of the cell performance.

Viscosity Measurement: Viscosities of the electrolytes were measured at room temperature using an Ostwald viscometer (Sibata Scientific Technology, Japan) with a capillary diameter of 0.75 mm. The temperature of the electrolyte in the viscometer was controlled constant by a circulating water bath (Sibata Scientific Technology, Japan).

Cell performance testing: The pouch cells first went through 4 charge/discharge cycles of formation protocol at C/20 in between 3.0 to 4.2 V. Following formation cycling, the cells were degassed and resealed under vacuum. The same pressure of 4 psi was applied back on the cells in between two Al plates. The cell performance test was carried out on the battery cycler (Maccor Series 4000) at 30 °C. The cells were cycled between 2.8 and 4.2 V with a constant voltage holding at 4.2 V (trickle charging). A total time limit was imposed to guarantee that the duration of the charging step did not exceed the intended time for each C rate (15 min for 4C charging, 20 min for 3C, and 1 hour for 1C charging). Both NMC622 cathode and graphite anode electrodes were punched from aged NMC622 pouch cells (fully discharged to 2.5 V) after disassembling in the Ar-filled glove box.

XPS characterization: XPS characterization of the surface chemistry on negative electrodes were conducted on a PHI Versa Probe III scanning XPS microscope, with monochromatic Al K-alpha X-ray source (1486.6 eV). Samples were prepared in an Ar-filled glove box then transferred to the XPS ultra-high vacuum chamber via a transfer vessel. XPS spectra were acquired with 200 mm/50 W/15 kV X-ray settings and dual-beam charge neutralization. All binding energies were referenced to CeC peak at 284.8 eV. The atomic ratios of elements were determined from the integrated intensity of elemental photoemission features corrected by each element's relative atomic sensitivity factors using CasaXPS.

Neutron powder diffraction (NPD): To probe the structural evolution of cycled electrodes, NPD characterizations were implemented on cycled NMC622 cathode and graphite anode at the NOMAD beamline of Spallation Neutron Source (SNS) of ORNL. NMC622 cathode and graphite anode materials were first rinsed with fresh DMC 3 times and then vacuum dried in the antechamber of the glovebox. Collected data was further processed using Rietveld refinement via Topas V6 [17].

Results and discussions

Figure 1 shows the conductivity and viscosity of the LiFSI electrolyte with different concentrations. The viscosities of the electrolytes show a monotonically increasing trend with increasing Li salt concentration, with 0.75 mol/L exhibiting the smallest viscosity of ~ 1.8 mPa s and 2.0 mol/L with the highest ~ 5.6 mPa s. This phenomenon can be ascribed to the decrease of solvent in the binary solution of the salt and the solvent [18,19]. The behavior of conductivities with changes of Li ion concentration can be satisfactorily explained similar to previous reports [7,18,20,21]. The conductivity increases initially due to the increase of dissociated ions with higher Li ion concentration. The electrolyte at 1.5 M achieved the highest conductivity. However, the conductivity drops with further increase of Li ion concentration. This is attributed to the reduction of dissociated ions because less solvent molecules are available to solvate Li ions and thus more ion-pairing occurred in the electrolyte [18]. These ion-pairing cease to contribute to ionic conductivity.

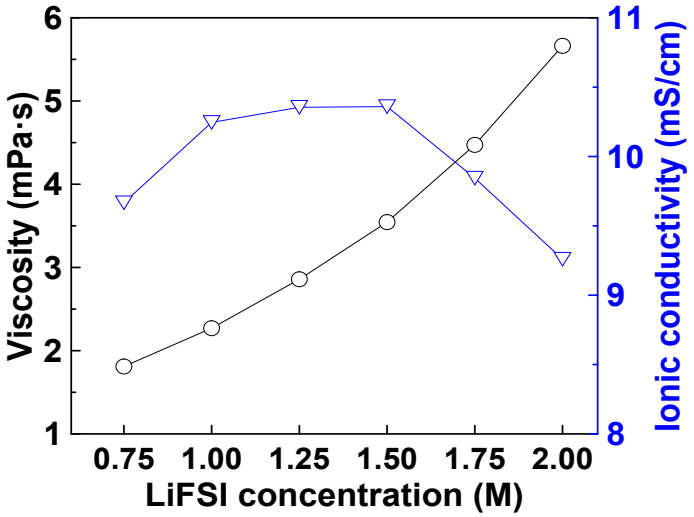

Figure 1. Conductivities and viscosity of the electrolytes with different Li salt concentration.

Figure 2 summarizes the rate performance of NMC622/graphite pouch cells filled with the different concentration electrolytes at charging rate (charging time) of C/3 (3 hours), 1C (1 hour), 2C (30 minutes) to 4C (15 minutes). At charging rate of C/3, all cells retains ~ 95% capacity except the one with 2.00 M electrolyte (capacity retention of ~ 92.5%). With the increase of charge rate (shortening of charging time), the difference in attainable capacity from different concentration electrolytes becomes more obvious. At 4C rate, 2.00 M electrolyte shows the least attainable

capacity followed by 1.75 M electrolyte. This can be ascribed to the high viscosity and low ion conductivity in increased concentration. For electrolyte concentration from 0.75 M to 1.50 M, the cells show similar capacities from charging rate of C/3 to 4C. This can be accredited to good balance of viscosity and ionic conductivity in these electrolyte concentrations.

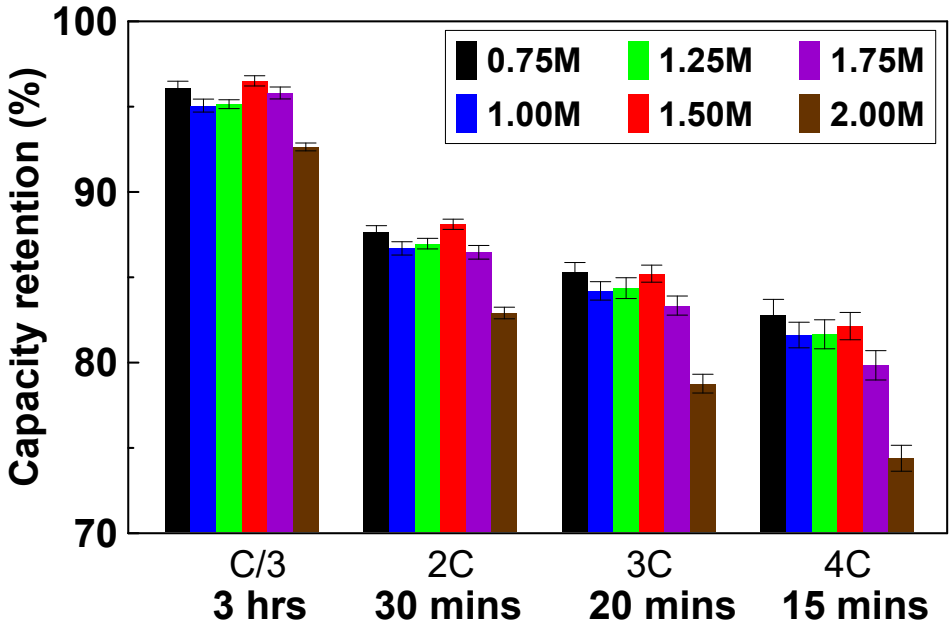

Figure 2: Discharge capacity (compared the capacity at rate of ±C/10) of pouch cells filled with different concentration electrolyte and charged at different C rate (time).

Figure 3a and b shows the long-term cycling performance and the mean charge voltage of pouch cells with different concentration electrolytes at charging rate of 4C. The cell with 0.75 M electrolyte shows poor cycling performance with less than 70% capacity attainable after 200 cycles. The cycling performance is gradually improved with the increase of electrolyte concentration. The poor cycling performance associated with low electrolyte concentration is probably related to the polarization and Li ion depletion during fast charging. As elaborated in previous work by Du et al. [2], lower concentration is prone to Li ion depletion at higher rate. The Li ion depletion can lead to metallic Li plating and thus more capacity fading from increased side reactions [22]. This is supported by the mean charge voltage changes over cycling in Figure 3b. although the charge voltage is similar for electrolyte concentration from 0.75 M to 1.5 M, the rapid increase of charge voltage for 0.75M indicates the increase of internal cell resistance. This could be ascribed to Li ion depletion and low ionic conductivity from the concentration gradient building up. This could also be ascribed to the SEI layer growth from electrolyte decomposition[23,24],

which indicates thicker SEI on graphite and/or plated Li are formed in lower concentration electrolyte gradually over cycling. With the increase initial Li ion concentration, the mean charge voltage become more stable over cycling. The cell with 1.50 M electrolyte shows the best performance with the highest attainable capacity and stability in 200 cycles. The cycling performance for 1.75 M and 2.00 M electrolyte are satisfactory except the attainable capacity through the 200 cycles are lower than the one at 1.50 M. This is due to the limited ion conductivity and highest viscosity in high concentrations. The gradual increase of the capacity with cycling number for 2.00 M electrolyte might be ascribed to the slow wetting of the cell from the high viscosity of the electrolyte. This is also supported by the fact that the mean charge voltage decreases over cycling in 1.75 M and 2.00 M electrolyte, which is attributed to the improvement of internal resistance and reduction of polarization.

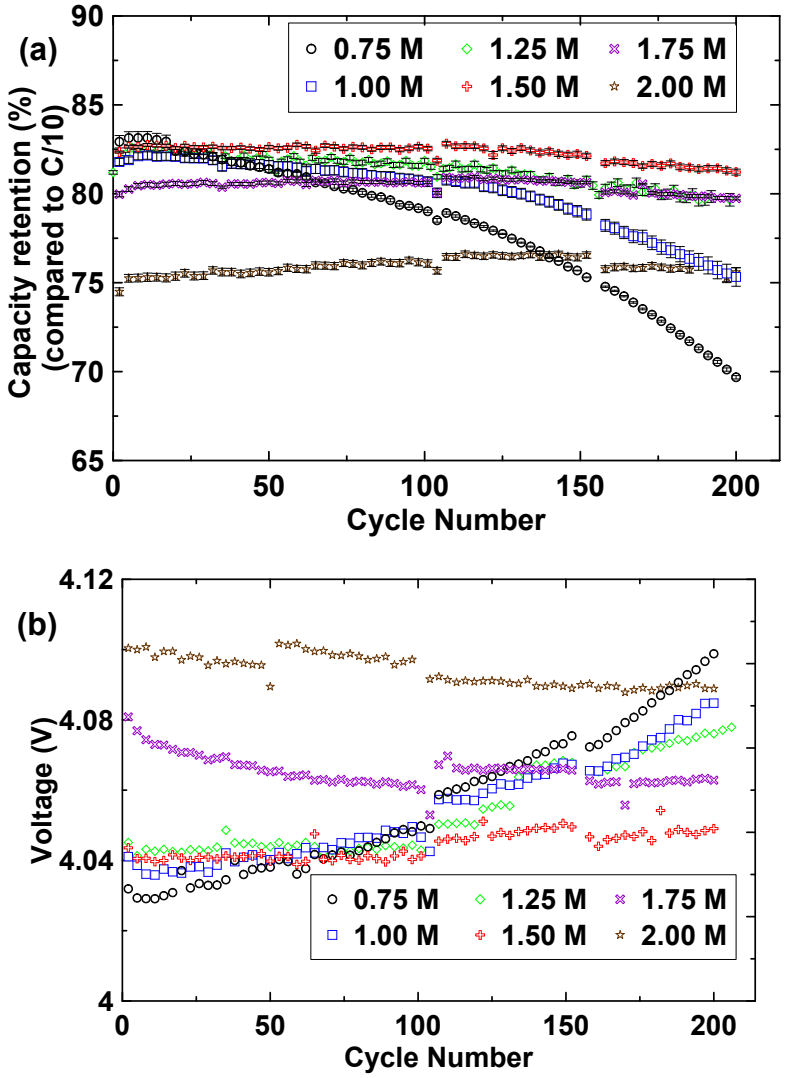

Figure 3. Long-term cycling (a) capacity and (b) mean charge voltage of the pouch cells filled with different concentration electrolytes cycled at 4C charging rate and discharge at 1C rate.

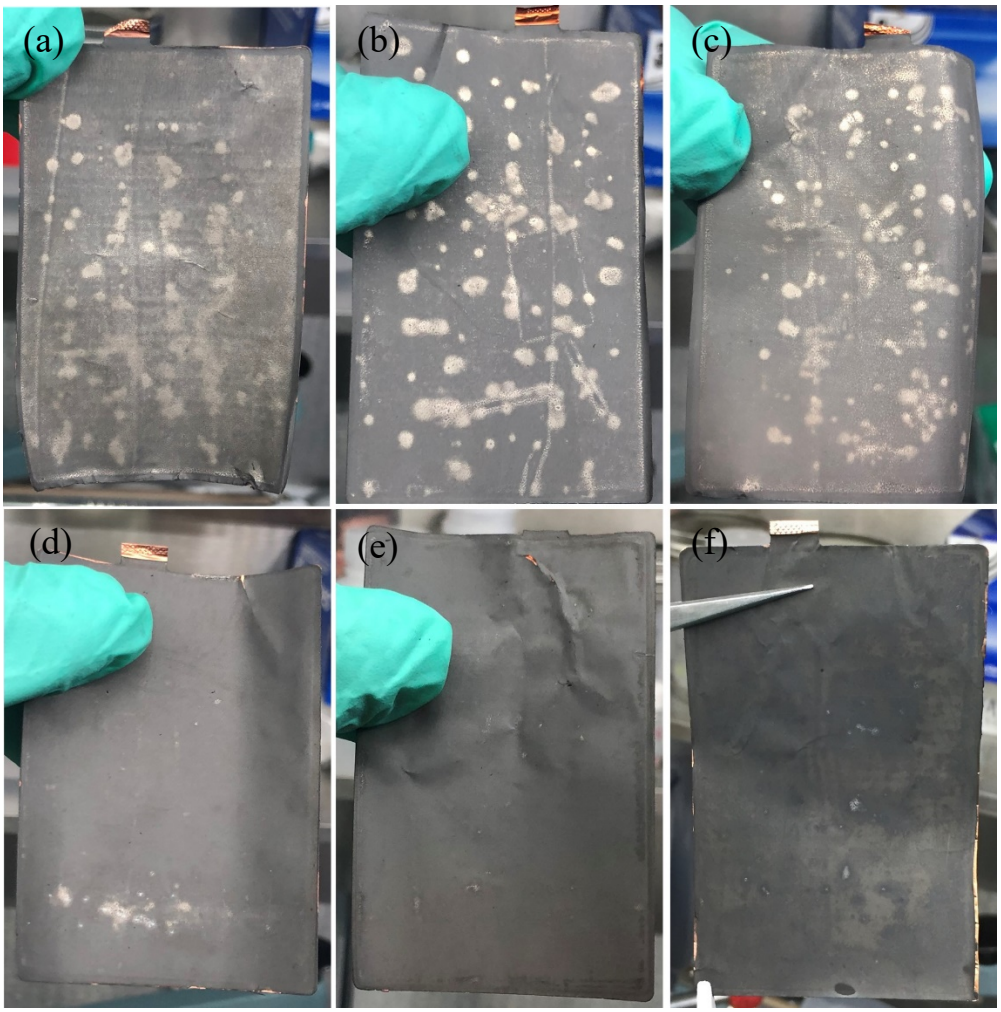

Figure 4. Li plating on graphite electrodes after 200 fast charging cycles with different concentration electrolytes: (a) 0.75 M, (b) 1.00 M, (c) 1.25 M, (d) 1.50 M, (e) 1.75 M, (f) 2.00 M.

Figure 4 shows the optical images of graphite electrode after 200 fast charging cycles to observe Li plating in the cells. For electrolyte with concentrations of 0.75 M, 1.00 M and 1.25 M (Figure 4a-c), specks of Li plating can be clearly seen across the graphite electrode surface. Interestingly, the Li plating distribution on electrode surface is geometrically different from previous report by Gallagher et al. where the Li plating is mainly one large area at the center [25]. The cell dimension here in this study nearly triples the size in Ref [25]. A more uniform pressure distribution on the pouch cells in this report may lead to randomly distributed Li plating spots. The Li plating in the Figure 4a-c can be easily related to the cycling performance as Li plating has been identified as an accelerating factor for capacity fading [26]. It is interesting that 1.50 M electrolyte in Figure 4d

shows greatly alleviated Li plating issue with a much smaller area of Li plating observed. No Li plating is observed for 1.75 M and 2.00 M electrolyte, which is mainly due to the avoidance of Li ion depletion in high salt concentration electrolyte. Figure 4d-e is consistent to the excellent cycling performance for electrolyte concentrations of 1.50 M, 1.75 M, and 2.00 M when Li plating can be avoided during fast charging.

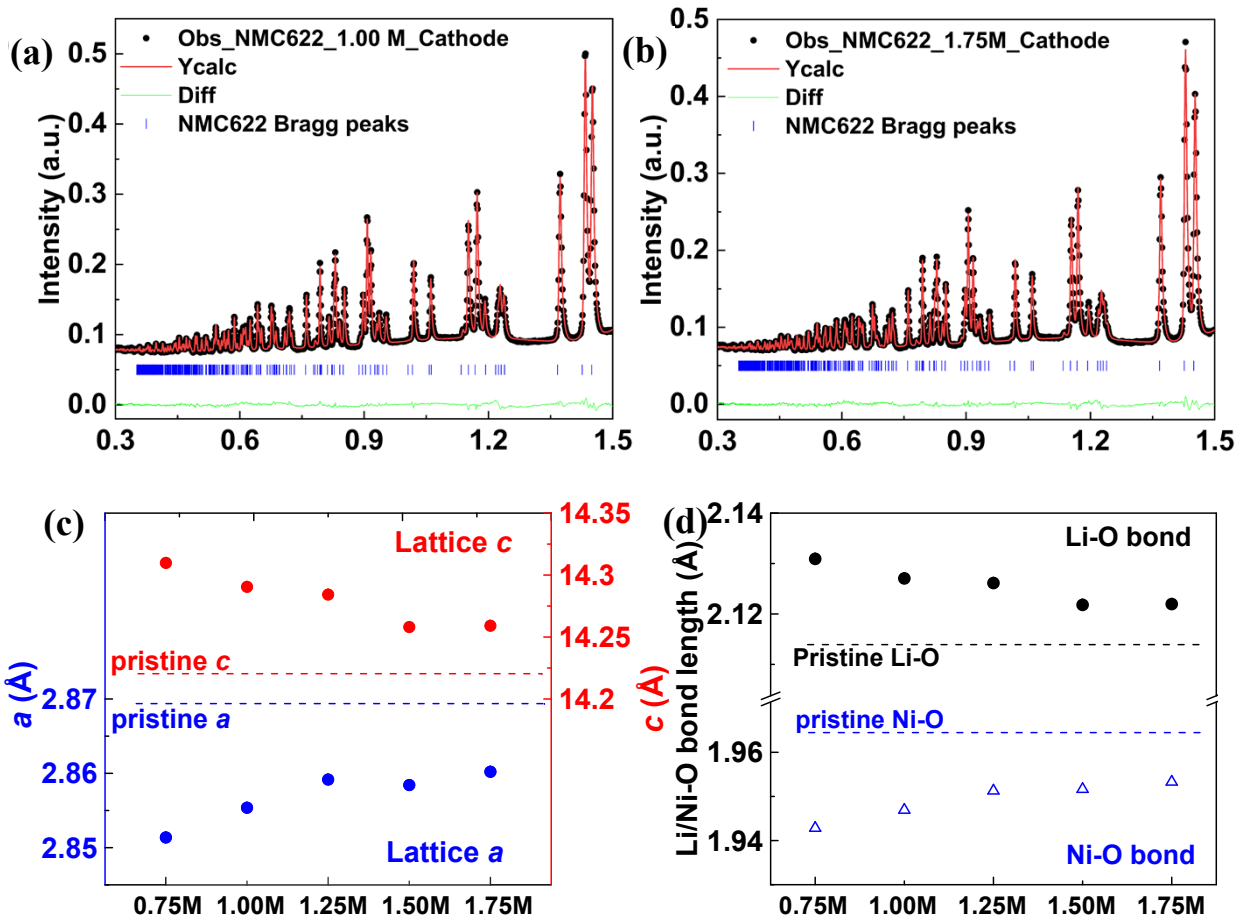

Figure 5. (a and b) The Rietveld refinement results for NMC622 samples after 200 fast charging cycles with electrolyte concentration of 1.00 M and 1.75 M; (c) lattice parameters *a* and *c*; (d) Li-O and Ni-O bond lengths.

Figure 5 shows the NPD analysis of NMC622 cathode after 200 fast charging cycles. Figure 5a and b show exemplary (1.00 M and 1.75 M) diffraction patterns and Rietveld refinement to obtain the lattice parameters. Previous studies indicated that NMC622 would maintain its original $R\bar{3}m$ crystal structure while lattice parameters *a* and *c* evolve due to the loss of active Li within NMC622 after long term cycling [27,28]. Lattice parameter *a* decreases when Li ions are lost in the layered structure. This is because the oxidation state of transition metal (TM) cations increases to balance

the charges lost by the loss of Li ions, leading to the decrease of their ionic radii and increase of the covalency between TM cations (e.g., Ni and Co) and ligand oxygen anion. Lattice c increases when Li ions are lost in cathode which is due to the reduction of the screening effect between adjacent oxygen planes, and thus leading to the increase of electrostatic repulsion between oxygen planes [8]. Figure 5c shows the decrease of *a* and increase of *c* in all samples compared to the pristine values. This suggests the loss of active Li in all electrodes. Although a quantitative analysis of the Li loss in cathode structure is difficult, comparison among electrodes from different concentration electrolytes shows a general trend that higher concentration electrolyte has less Li loss because *a* and *c* are closer to the pristine values. Similar trend is also found in the changes of Li-O and Ni-O bond lengths as shown in Figure 5d. Li loss from the structure is indicated by the decrease of Ni-O bond and the increase of Li-O bond [28]. With the increase of electrolyte concentration, the deviation of Li-O and Ni-O bond lengths from the pristine values diminishes, indicating less Li loss in the cells.

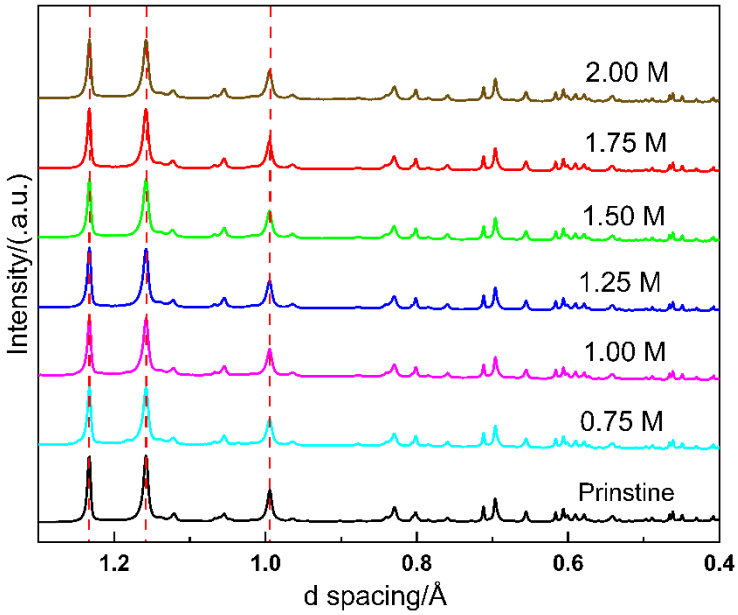

Figure 6. NPD patterns of graphite electrodes after 200 fast charging cycles.

Figure 6 shows the NPD of graphite electrodes after 200 fast charging cycles. No peak shifting or intensity changes is observed compared to the pristine graphite electrode. This suggests the structure of graphite is well maintained and there is little residual Li in between graphene layers after the cells were fully discharged. The whereabouts of the lost active Li from the cathode structure are the dead Li plating and the side reactions at the anode/electrolyte interfaces.

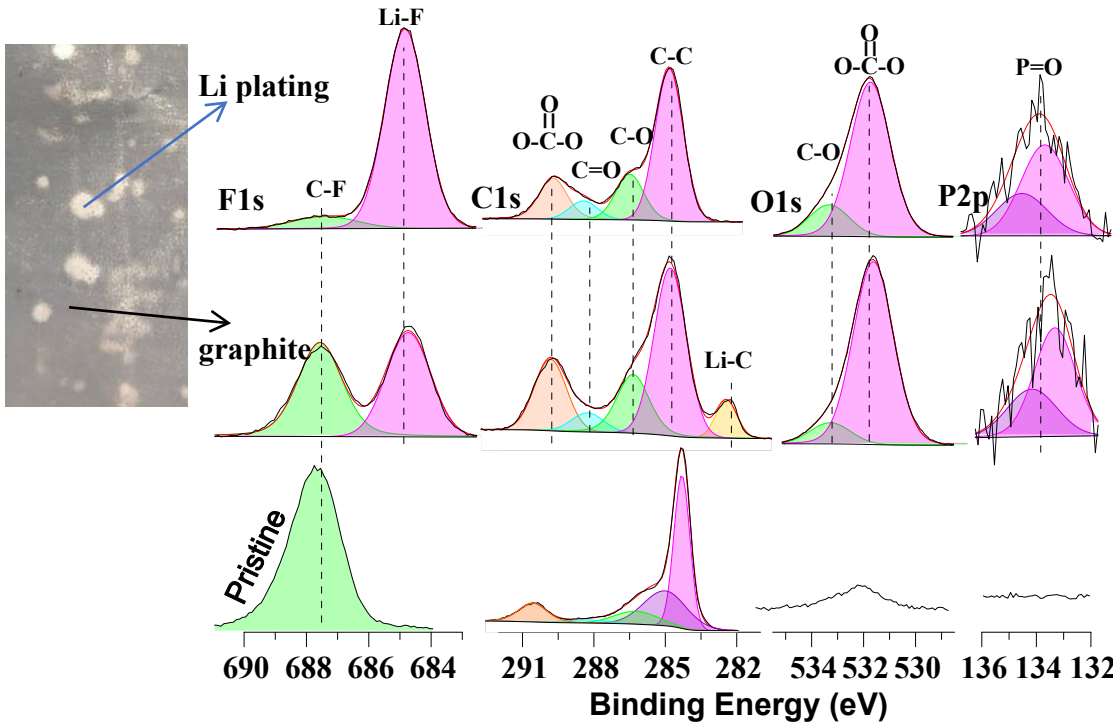

Figure 7. XPS results on graphite electrodes after 200 fast charging cycles with two different areas of Li plating area and graphite area without Li plating. The electrolyte concentration is 1.25 M.

Figure 7 shows the XPS analysis of the interfaces between graphite and electrolyte. Two different areas of interest were studied with one on the plated Li and the other one on graphite without Li plating. It is well known that the solid electrolyte interphase (SEI) on graphite electrodes consists of both organic compounds (such as $(CH_2OCO_2Li)_2$ (lithium ethylene decarbonate, LEDC), other organic carbonates (R_2CO_3), polyethylene glycol (PEO) oligomer) and inorganic compounds (such as Li_2CO_3, LiF, Li_2O, $LiPF_xO_y$ and Li_xPF_y) [29,30]. The assignments for peaks in the F 1s, C 1s O 1s and P 2p have been summaries in our previous report [8]. Compared to pristine graphite electrode surface, both plated Li and graphite areas show rich features of SEI components from all 4 spectra, which is accumulated from the repeated charge/discharge cycles. In F1s spectra, only C-F is observed in pristine sample which can be assigned to the C-F in PVDF binder. Li-F is detected in cycled graphite electrode, which can be attributed to LiF from the decomposition of Li salt [31]. The fact that C-F peak intensity is much smaller than that of Li-F in Li plating area compared to graphite area indicates the Li plating occurs on the surface of graphite. The plated Li increases the local thickness of the cell. This mechanical deformation would induce local inhomogeneous pressure[32], which can lead to inhomogeneous ion flux distributions and cause more lithium plating [33]. For C1s, O1s and P2p, similar spectra are noticed for Li plating area

and graphite area, which can be assigned to the side reaction products from Li salt and solvents. One exception is the Li-C bond at ~ 282 eV for C1s in graphite area, which can be ascribed to Li-C bond from residual Li_xC intercalation compounds. The residual Li in graphite structure must be minimal as it was not observed in the NPD characterization.

These above results suggest that the concentrations of electrolyte have a significant effect on the fast charging performance of Li-ion cells. As Li salt concentration increases, many properties of electrolyte will change, such as solvation structure, ionic transport properties (viscosity, ion conductivity, transference number and Li ion concentration gradient thus formed), and SEI formed at anode side (compositions, morphology). In this study, fast charging testing of Li-ion cells demonstrated electrolyte concentration should be optimized in a given Li-ion cell setting. Increasing concentration can alleviate Li ion depletion issue during high charging rate while ionic conductivity can decrease from increase of viscosity and ion pairing. 1.50 M is shown here to be the optimized concentration for ~3 mAh/cm^2 loading NMC622/graphite cells. More systematic studies can help to gain deeper understanding on improved long term cycling performance under fast charging.

Conclusion

The effects of different Li salt concentrations of (LiFSI/$LiPF_6$ 9/1 mole ratio) in carbonate electrolyte on fast charging performance were studied in NMC622/graphite pouch cells. With the increase of concentration, the viscosity of the electrolyte increases, while the conductivity increases first and then decreases due to the association between anions and cation. High concentration electrolyte (1.75 M and 2.00 M) shows less attainable capacity during fast charging compared to low concentration ones. However, low concentration electrolyte shows faster capacity fading in long term cycling. With the increase of concentration, the cycling performance is improved. Electrolyte at 1.5 M shows the best overall performance with high attainable capacity and excellent cycling performance at 4C charging rate. The post-mortem analysis on Li plating with different electrolyte concentrations aligns well with the cycling performance. NPD characterization also demonstrated that active Li loss in cathode decreases after 200 fast charging cycles with the increase of electrolyte concentrations. This study suggests that it is desirable to optimize electrolyte concentration with a given cell configuration and areal loading for fast charging.

Acknowledgement

This research at Oak Ridge National Laboratory, managed by UT Battelle, LLC, for the U.S. Department of Energy (DOE) under contract DE-AC05-00OR22725, was sponsored by the Laboratory Directed Research and Development Program and by the Office of Energy Efficiency and Renewable Energy (EERE) Vehicle Technologies Office (VTO) (Technology Manager: Brian Cunningham). Neutron diffraction in this research used resources at the Spallation Neutron Source, a DOE Office of Science User Facility operated by the Oak Ridge National Laboratory. The XPS study was performed at the Surface Analysis Laboratory in Department of Chemistry at Virginia Tech, which is supported by the National Science Foundation under Grant No. CHE-1531834.

References

[1] S. Ahmed, I. Bloom, A.N. Jansen, T. Tanim, E.J. Dufek, A. Pesaran, A. Burnham, R.B. Carlson, F. Dias, K. Hardy, M. Keyser, C. Kreuzer, A. Markel, A. Meintz, C. Michelbacher, M. Mohanpurkar, P.A. Nelson, D.C. Robertson, D. Scoffield, M. Shirk, T. Stephens, R. Vijayagopal, J. Zhang, Enabling fast charging – A battery technology gap assessment, J. Power Sources. 367 (2017) 250–262. doi:10.1016/j.jpowsour.2017.06.055.

[2] Z. Du, D.L. Wood, C. Daniel, S. Kalnaus, J. Li, Understanding limiting factors in thick electrode performance as applied to high energy density Li-ion batteries, J. Appl. Electrochem. 47 (2017) 405–415. doi:10.1007/s10800-017-1047-4.

[3] C. Uhlmann, J. Illig, M. Ender, R. Schuster, E. Ivers-Tiffée, In situ detection of lithium metal plating on graphite in experimental cells, J. Power Sources. 279 (2015) 428–438. doi:10.1016/j.jpowsour.2015.01.046.

[4] S.S. Zhang, K. Xu, T.R. Jow, Study of the charging process of a LiCoO2-based Li-ion battery, J. Power Sources. 160 (2006) 1349–1354. doi:10.1016/j.jpowsour.2006.02.087.

[5] J.C. Burns, D.A. Stevens, J.R. Dahn, In-Situ Detection of Lithium Plating Using High Precision Coulometry, J. Electrochem. Soc. 162 (2015) A959–A964. doi:10.1149/2.0621506jes.

[6] E.R. Logan, J.R. Dahn, Electrolyte Design for Fast-Charging Li-Ion Batteries, Trends Chem. 2 (2020) 354–366. doi:10.1016/j.trechm.2020.01.011.

[7] Z. Du, D.L. Wood, I. Belharouak, Enabling fast charging of high energy density Li-ion cells with high lithium ion transport electrolytes, Electrochem. Commun. 103 (2019) 109–113. doi:10.1016/j.elecom.2019.04.013.

[8] X. Wu, T. Liu, Y. Bai, X. Feng, M.M. Rahman, C.-J. Sun, F. Lin, K. Zhao, Z. Du, Effects of solvent formulations in electrolytes on fast charging of Li-ion cells, Electrochim. Acta. 353 (2020) 136453. doi:10.1016/j.electacta.2020.136453.

[9] A.M. Colclasure, A.R. Dunlop, S.E. Trask, B.J. Polzin, A.N. Jansen, K. Smith, Requirements for Enabling Extreme Fast Charging of High Energy Density Li-Ion Cells

while Avoiding Lithium Plating, J. Electrochem. Soc. 166 (2019) A1412–A1424. doi:10.1149/2.0451908jes.

[10] J. Newman, K.E. Thomas-Alyea, Electrochemical Systems, 3rd ed., John Wiley & Sons, Ltd, New York, 2004.

[11] X. Wu, Z. Du, Study of the corrosion behavior of LiFSI based electrolyte for Li-ion cells, Electrochem. Commun. 129 (2021) 107088. doi:10.1016/j.elecom.2021.107088.

[12] L.O. Valøen, J.N. Reimers, Transport Properties of LiPF[sub 6]-Based Li-Ion Battery Electrolytes, J. Electrochem. Soc. 152 (2005) A882. doi:10.1149/1.1872737.

[13] D.Y. Wang, J.C. Burns, J.R. Dahn, A Systematic Study of the Concentration of Lithium Hexafluorophosphate (LiPF6) as a Salt for LiCoO2/Graphite Pouch Cells, J. Electrochem. Soc. 161 (2014) A1278–A1283. doi:10.1149/2.0611409jes.

[14] R. Petibon, L. Madec, D.W. Abarbanel, J.R. Dahn, Effect of LiPF6 concentration in Li[Ni0.4Mn0.4Co0.2]O2/graphite pouch cells operated at 4.5 V, J. Power Sources. 300 (2015) 419–429. doi:https://doi.org/10.1016/j.jpowsour.2015.09.090.

[15] R. Zhao, S. Zhang, J. Gu, J. Liu, Modeling the electrochemical behaviors of charging Li-ion batteries with different initial electrolyte salt concentrations, Int. J. Energy Res. 40 (2016) 1085–1092. doi:https://doi.org/10.1002/er.3502.

[16] D.J. Xiong, T. Hynes, J.R. Dahn, Dramatic Effects of Low Salt Concentrations on Li-Ion Cells Containing EC-Free Electrolytes, J. Electrochem. Soc. 164 (2017) A2089–A2100. doi:10.1149/2.1381709jes.

[17] A.A. Coelho, TOPAS and TOPAS-Academic: An optimization program integrating computer algebra and crystallographic objects written in C++, J. Appl. Crystallogr. 51 (2018) 210–218. doi:10.1107/S1600576718000183.

[18] M.S. Ding, K. Xu, S.S. Zhang, K. Amine, G.L. Henriksen, T.R. Jow, Change of Conductivity with Salt Content, Solvent Composition, and Temperature for Electrolytes of LiPF[sub 6] in Ethylene Carbonate-Ethyl Methyl Carbonate, J. Electrochem. Soc. 148 (2001) A1196. doi:10.1149/1.1403730.

[19] K. Kondo, M. Sano, A. Hiwara, T. Omi, M. Fujita, A. Kuwae, M. Iida, K. Mogi, H. Yokoyama, Conductivity and Solvation of Li + Ions of LiPF 6 in Propylene Carbonate Solutions, J. Phys. Chem. B. 104 (2000) 5040–5044. doi:10.1021/jp000142f.

[20] E.R. Logan, E.M. Tonita, K.L. Gering, J. Li, X. Ma, L.Y. Beaulieu, J.R. Dahn, A Study of the Physical Properties of Li-Ion Battery Electrolytes Containing Esters, J. Electrochem. Soc. 165 (2018) A21–A30. doi:10.1149/2.0271802jes.

[21] M.S. Ding, T.R. Jow, Conductivity and Viscosity of PC-DEC and PC-EC Solutions of LiPF[sub 6], J. Electrochem. Soc. 150 (2003) A620. doi:10.1149/1.1566019.

[22] H.J. Chang, A.J. Ilott, N.M. Trease, M. Mohammadi, A. Jerschow, C.P. Grey, Correlating Microstructural Lithium Metal Growth with Electrolyte Salt Depletion in Lithium Batteries Using 7Li MRI, J. Am. Chem. Soc. 137 (2015) 15209–15216. doi:10.1021/jacs.5b09385.

[23] E. Peled, The Electrochemical Behavior of Alkali and Alkaline Earth Metals in Nonaqueous Battery Systems—The Solid Electrolyte Interphase Model, J. Electrochem. Soc. 126 (1979) 2047–2051. doi:10.1149/1.2128859.

[24] A.J. Smith, J.C. Burns, X. Zhao, D. Xiong, J.R. Dahn, A High Precision Coulometry Study of the SEI Growth in Li/Graphite Cells, J. Electrochem. Soc. 158 (2011) A447. doi:10.1149/1.3557892.

[25] K.G. Gallagher, S.E. Trask, C. Bauer, T. Woehrle, S.F. Lux, M. Tschech, P. Lamp, B.J. Polzin, S. Ha, B. Long, Q. Wu, W. Lu, D.W. Dees, A.N. Jansen, Optimizing Areal Capacities through Understanding the Limitations of Lithium-Ion Electrodes, J. Electrochem. Soc. 163 (2016) A138–A149. doi:10.1149/2.0321602jes.

[26] X.-G. Yang, Y. Leng, G. Zhang, S. Ge, C.-Y. Wang, Modeling of lithium plating induced aging of lithium-ion batteries: Transition from linear to nonlinear aging, J. Power Sources. 360 (2017) 28–40. doi:10.1016/j.jpowsour.2017.05.110.

[27] C.H. Shen, S.Y. Shen, F. Fu, C.G. Shi, H.Y. Zhang, M.J. Pierre, H. Su, Q. Wang, B. Bin Xu, L. Huang, J.T. Li, S.G. Sun, New insight into structural transformation in Li-rich layered oxide during the initial charging, J. Mater. Chem. A. 3 (2015) 12220–12229. doi:10.1039/c5ta01849h.

[28] J. Liu, Z. Du, X. Wang, S. Tan, X. Wu, L. Geng, B. Song, P.-H. Chien, S.M. Everett, E. Hu, Anionic redox induced anomalous structural transition in Ni-rich cathodes, Energy Environ. Sci. 14 (2021) 6441–6454. doi:10.1039/D1EE02987H.

[29] G. Zhuang, Y. Chen, P.N. Ross, The Reaction of Lithium with Dimethyl Carbonate and Diethyl Carbonate in Ultrahigh Vacuum Studied by X-ray Photoemission Spectroscopy, Langmuir. 15 (1999) 1470–1479. doi:10.1021/la980454y.

[30] R. Dedryvère, H. Martinez, S. Leroy, D. Lemordant, F. Bonhomme, P. Biensan, D. Gonbeau, Surface film formation on electrodes in a LiCoO2/graphite cell: A step by step XPS study, J. Power Sources. 174 (2007) 462–468. doi:10.1016/j.jpowsour.2007.06.033.

[31] P. Niehoff, M. Winter, Composition and growth behavior of the surface and electrolyte decomposition layer of/on a commercial lithium ion battery LixNi 1/3Mn1/3Co1/3O2 cathode determined by sputter depth profile X-ray photoelectron spectroscopy, Langmuir. 29 (2013) 15813–15821. doi:10.1021/la403276p.

[32] T. Waldmann, S. Gorse, T. Samtleben, G. Schneider, V. Knoblauch, M. Wohlfahrt-Mehrens, A Mechanical Aging Mechanism in Lithium-Ion Batteries, J. Electrochem. Soc. 161 (2014) A1742–A1747. doi:10.1149/2.1001410jes.

[33] G. Fuchs, L. Willenberg, F. Ringbeck, D.U. Sauer, Post-Mortem Analysis of Inhomogeneous Induced Pressure on Commercial Lithium-Ion Pouch Cells and Their Effects, Sustainability. 11 (2019) 6738. doi:10.3390/su11236738.